Fall 12-2020

Constraining Respired Carbon Storage in the Eastern Tropical Pacific Over the Last 25 Thousand Years Using Benthic Foraminiferal Boron/Calcium Ratios

Brian James Close
Old Dominion University, bclos001@odu.edu

CONSTRAINING RESPIRED CARBON STORAGE IN THE EASTERN TROPICAL PACIFIC OVER THE LAST 25 THOUSAND YEARS USING BENTHIC FORAMINIFERAL BORON/CALCIUM RATIOS

By

Brian James Close
B.S. August 2017, West Virginia University

A Thesis Submitted to the Faculty of
Old Dominion University in Partial Fulfillment of the
Requirements for the Degree of

MASTER OF SCIENCE

OCEAN AND EARTH SCIENCES

OLD DOMINION UNIVERSITY
December 2020

Approved by:

Matthew Schmidt (Director)

David Burdige (Member)

Peter Sedwick (Member)

ABSTRACT

CONSTRAINING RESPIRED CARBON STORAGE IN THE EASTERN TROPICAL PACIFIC OVER THE LAST 25 THOUSAND YEARS USING BENTHIC FORAMINIFERAL BORON/CALCIUM RATIOS

Brian James Close
Old Dominion University, 2020
Director: Dr. Matthew Schmidt

The storage of inorganic carbon in the deep Pacific Ocean is thought to play an important role in regulating both glacial-interglacial and millennial-scale atmospheric CO_2 concentrations (Broecker and Barker 2007; Sigman et al., 2010). A recent study by Loveley et al. (2017) showed that sedimentary authigenic uranium (aU) concentrations, a proxy for suboxic bottom-water conditions, increased significantly in the Eastern Equatorial Pacific (EEP) during the Last Glacial Maximum (LGM, 18 kyr – 23 kyr). If this is correct, the low-oxygen, CO_2-rich waters would also have a lower pH and a lower carbonate ion concentration ($[CO_3^{2-}]$). Yu and Elderfield (2007) showed that the boron to calcium (B/Ca) ratio in the benthic foraminifera *C. wuellerstorfi* is a reliable proxy for reconstructing bottom water $[CO_3^{2-}]$. Here I present new constraints on deep ocean carbon storage over the last 25 kyr in the EEP using new benthic foraminiferal B/Ca-$[CO_3^{2-}]$ reconstructions from four cores at a range of depths from within and outside the Panama Basin. These four new records all reveal lower glacial $[CO_3^{2-}]$, with the largest LGM-Holocene difference coming from core MV1014-02-17JC (17JC) (00°10.83'S, 85°52.00'W; 2.9 km water depth) inside the Panama Basin. New depth profiles of glacial carbon storage in the region show that respired CO_2 storage outside the Panama Basin was relatively homogenous while inside the basin there was a gradient of increasing CO_2 storage with depth

from 2.2 km down to 2.9 km. A new sub-millennial scale record shows that during the last deglaciation (18 kyr - 11 kyr), waters inside the Panama Basin experienced two large increases in respired CO_2 storage during Heinrich Stadial 1 and the Younger Dryas. Finally, intra-core proxy comparisons of ^{232}Th (a dust flux proxy), excess barium (a paleoproductivity proxy), and aU from 17JC and MV1014-02-8JC (8JC) (6°14'N, 86°2'W; 2 km water depth) illustrate that two different mechanisms likely influenced CO_2 storage in the region. For 8JC, a poorly ventilated Pacific wide water mass was likely the source for the lower glacial [CO_3^{2-}] at its core location. While for 17JC, in addition to the previously noted poorly ventilated water mass influence, respired CO_2 storage at this core location was further enhanced by millennial scale increases in export production. By sequestering carbon away from the atmosphere and surface ocean, deep waters in the Panama Basin and in the greater EEP region likely played an important role in lowering glacial atmospheric CO_2.

This thesis is dedicated to Kinsey M. Reed,
she inspires me each day to be the best version of myself

AKNOWLEDGMENTS

There are many people who have contributed to the completion of this thesis. I extend thanks to my fellow lab mates, Lenzie Ward, Colton Watkins, and Ryan Glaubke for always making paleoceanography enjoyable. Thanks to Bettina Sohst for her assistance with running our samples on the ICP-MS (sorry for possibly breaking “sippy”). Unending thanks to Dr Jennifer Hertzberg for her patience with guiding me through our lab procedures and for her impeccable editing skills. I thank Dr Matthew Schmidt for taking a chance several years ago and having faith that I could handle a project of this magnitude. Finally, a special thanks to my parents, Jim and Susan Close, who have always supported my ambitions and believed in what I could achieve.

NOMENCLATURE

Al/Ca	Aluminum to Calcium Ratio, mmol/mol
AAIW	Antarctic Intermediate Water
UCDW	Antarctic Upper Circumpolar Deep-Water
aU	Authigenic Uranium, ppm
BA	Bølling–Allerød
B/Ca	Boron to Calcium Ratio, µmol/mol
DIC	Dissolved Inorganic Carbon, µmol/kg
EEP	Eastern Equatorial Pacific
Fe/Ca	Iron to Calcium Ratio, mmol/mol
xsBa	Excess Barium Mass Accumulation Rate, mg cm^{-2} kyr^{-1}
HS1	Heinrich Stadial 1
HS2	Heinrich Stadial 2
HNLC	High Nutrient Low Chlorophyll
ITCZ	Intertropical Convergence Zone
Kyr	Thousand Years
LGM	Last Glacial Maximum
LCDW	Lower Circumpolar Deep Water
Mg/Ca	Magnesium to Calcium Ratio, mmol/mol
Mn/Ca	Manganese to Calcium Ratio, mmol/mol
NPIW	North Pacific Intermediate Water
$[O_2]$	Oxygen Concertation, µmol/kg
PDW	Pacific Deep-Water

NOMENCLATURE

*p*CO2	Partial Pressure of Carbon Dioxide
^{232}Th	^{232}Thorium Mass Accumulation Rate, μg cm^{-2} kyr^{-1}
WOCE	World Ocean Circulation Experiment
YD	Younger Dryas

TABLE OF CONTENTS

Page

LIST OF TABLES

LIST OF FIGURES

I. INTRODUCTION

Antarctic ice core records show that atmospheric CO_2 concentrations and global temperatures are tightly coupled through at least the Pleistocene epoch (Bereiter et al., 2012). Although feedback mechanisms in the ocean-climate system likely controlled atmospheric CO_2 over this period, the ultimate driver of the pCO_2 variability remains a topic of debate in the paleoclimate community. One prevailing hypothesis postulates that a large pool of water enriched in respired carbon was present in the deep Pacific (below 3km) during glacial periods. Ventilation of this CO_2-rich water mass during the deglaciation theoretically drives the increase in atmospheric CO_2, which in turn warms the planet and brings an end to the ice ages (Sigman and Boyle, 2000). What is not known regarding this hypothesis is how and where the large volume of respired carbon was stored in the deep Pacific Ocean during glacial periods (Broecker et al., 2007).

A recent study by Loveley et al. (2017) presented new ^{232}Th, excess barium (xsBa), and authigenic uranium (aU) records from core MV1014-02-17JC (hereafter 17JC), collected near the equator just north of the Carnegie Ridge in the Panama Basin of the Eastern Equatorial Pacific (EEP) (00°10.83'S, 85°52.00'W; 2.9 km water depth; Figure 1). The ^{232}Th record was interpreted to indicate changes in dust flux to the EEP, while xsBa is a proxy for export productivity. Loveley et al. (2017) showed that dust flux in the EEP increased during cold climate periods in the North Atlantic, such as northern hemisphere Heinrich Events, due to a southward shift in the Intertropical Convergence Zone (ITCZ). Today, the EEP is a high nutrient low chlorophyll (HNLC) region, where productivity is limited by the micronutrient Fe. It was theorized that increased pulses of dust to the EEP likely relaxed the Fe limitation and led to increased productivity. Furthermore, most periods of increased dust flux corresponded to

elevated values of xsBa in 17JC, suggesting iron fertilization did indeed increase export production and biological pump strength when the ITCZ shifted southwards.

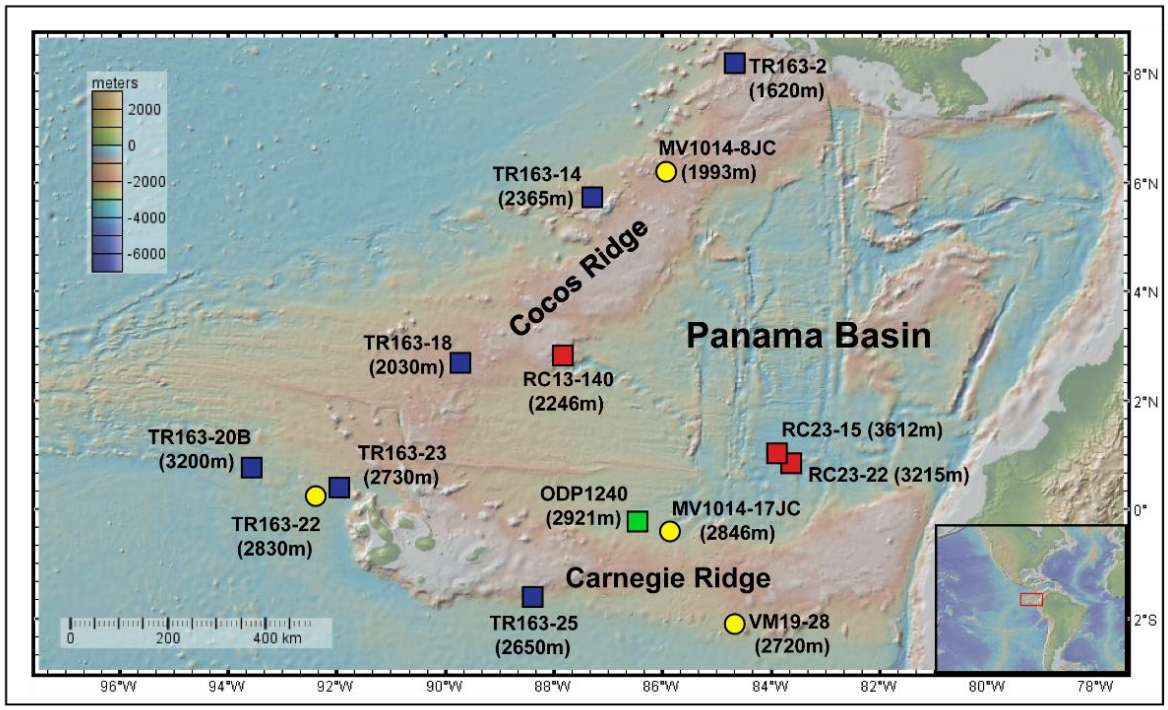

Figure 1: EEP Bathymetry. Regional Bathymetry of the EEP with locations of the four cores used in this study, (yellow circles) along with cores used by Umling and Thunell (2018) (blue squares), Doss and Marchitto (2013) (red squares), and De la Fuente et al. (2017) (green square).

Increased export production during periods of iron fertilization should have also affected local bottom water chemistry. As sinking organic carbon is ultimately remineralized, deep water [O_2], [CO_3^{2-}], and pH would decrease as [CO_2] increased. Loveley et al. (2017) showed that aU concentrations in 17JC reached their highest levels toward the end of the LGM, suggesting that bottom water O_2 concentrations inside the Panama Basin dropped to their lowest levels just as global atmospheric CO_2 concentrations reached their lowest levels over the last 25 kyr (Loveley et al., 2017). This is because uranium is reduced from U(VI), the soluble form uranyl carbonate,

to U(IV), which precipitates from solution as uranium oxide under suboxic conditions (Barnes and Cochran 1990).

The aU record in 17JC is similar to aU records from the Subarctic North Pacific (Galbraith et al., 2007), Western Pacific (Bradtmiller et al., 2010), EEP (Marcantonio et al., 2020), and Southern Ocean (Jaccard et al., (2016), suggesting the presence of a poorly ventilated, CO_2-rich deep-water mass that occupied a large volume of the deep Pacific during the LGM. Although the presence of low oxygen bottom waters during the glacial period might suggest the presence of a poorly ventilated, CO_2-rich deep-water mass in the glacial Pacific, localized suboxic conditions in the deep EEP could also have resulted from an increase in local productivity driven by Fe fertilization. If this is the case, the EEP may have been an important regional sink for the storage of respired carbon when atmospheric CO_2 concentrations were at their lowest.

As respired CO_2 concentrations increase in a parcel of water, the pH decreases and pushes the local DIC pool away from CO_3^{2-} (Emerson and Hedges, 2008). Therefore, this relationship can be used to assess variations in respired carbon storage in deep ocean water. By reconstructing variability in the [CO_3^{2-}] of a water mass through time, changes in local respired carbon storage can be inferred (Yu and Elderfield, 2007).

In order to reconstruct deep water [CO_3^{2-}] changes in the Pacific during the late Pleistocene, previous studies have analyzed B/Ca ratios in benthic foraminiferal tests (De la Fuente et al., 2017, Doss and Marchitto 2013, Umling and Thunell, 2018). Yu and Elderfield (2007) showed that the B/Ca ratio in benthic foraminiferal calcite is quantifiably linked with bottom water carbonate saturation state or $\Delta[CO_3^{2-}]$. Epifaunal benthic foraminifera calcify their tests using dissolved inorganic carbon from within the parcel of water they inhabit on the

seafloor (Yu and Elderfield, 2007). The two dominant boron species in the ocean are boric acid ($B(OH)_3$) and borate ion ($B(OH)_4^-$), with their concentrations varying relative to pH (Emmerson and Hedges, 2008). Foraminifera incorporate boron almost exclusively from the $B(OH)_4^-$ species, and $[B(OH)_4^-]$ decreases with decreasing bottom water pH (Yu and Elderfield, 2007). Therefore, foraminifera living in a water mass with a lower pH and lower $[CO_3^{2-}]$ have a lower B/Ca ratio in their calcite shell (Yu and Elderfield, 2007).

Since these initial studies, B/Ca ratios have been successfully used to quantify changes in deep-water $[CO_3^{2-}]$ at many locations (De la Fuente et al., 2017, Doss and Marchitto 2013, Umling and Thunell, 2018; Allen et al., 2015; Allen et al., 2020). Several previous studies from the EEP utilized this proxy and found generally lower glacial $[CO_3^{2-}]$ than modern. Nevertheless, the cause of this decrease remains an open question. Doss and Marchitto (2013) studied three cores from mid- to deep- depths inside the Panama Basin and found a decrease in glacial $[CO_3^{2-}]$ (Figure 1, red squares). They attribute this to a strengthening of low latitude productivity in the eastern tropical Pacific and subsequent sequestering of carbon to the deeper waters in the region. In addition, a study by Umling and Thunell (2018) used a group of cores from the surrounding western exterior of the Panama Basin and also found a decrease in $[CO_3^{2-}]$ during the LGM (Figure 1, blue squares). They concluded that there was an absence of evidence for enhanced EEP production during the LGM, and instead attributed the glacial $[CO_3^{2-}]$ decrease to respired carbon accumulation in a poorly ventilated water mass.

Nevertheless, Umling and Thunell (2018) saw consistently higher $[CO_3^{2-}]$ values in their study sites outside the Panama Basin as compared to Doss and Marchitto (2013)'s study sites inside the basin. This difference could indicate that the Panama Basin stored greater amounts of carbon relative to the rest of the Pacific due to its proximity to a terrestrial dust source leading to

Fe fertilization and the resulting enhanced export production. In addition, the presence of ridges surrounding the Panama Basin may act to further decrease ventilation of the deep waters inside the basin (Lonsdale and Malfait, 1974). To fully constrain the geographic influence of the Panama Basin on bottom water carbon storage, records from cores at similar depths from inside and outside the Panama Basin are needed. If [CO_3^{2-}] values are significantly lower at a similar depth inside the basin relative to outside, this would provide evidence of enhanced storage of carbon inside the Panama Basin.

In addition to the geographic influence of the Panama Basin on deep water carbon storage, the vertical extent of the deep carbon pool at the LGM remains a matter of debate. Doss and Marchitto (2013) constructed [CO_3^{2-}] records at three depths (2.2 km, 3.2 km and 3.6 km) inside the basin and found the largest LGM-Holocene difference in their cores at 3.2 km and 3.6 km, with the smallest difference from their core at 2.2 km. Umling and Thunell (2018) used cores with a depth range of 1.6 km to 3.2 km outside the Panama Basin and found that the largest LGM-Holocene difference was at 2.3 km and 3.2 km with cores from depths above 2 km showing higher LGM [CO_3^{2-}] compared to the Holocene. Hence, the vertical depth range of the hypothesized glacial Pacific carbon reservoir in the EEP remains unclear. In order to constrain the full vertical extent of the carbon pool at the LGM, a suite of cores spanning depths from ~2 km to ~3 km is needed. If [CO_3^{2-}] is lower during the LGM in this range of cores, then it provides support that the glacial reservoir was occupying a larger vertical extent than previously thought.

To determine if there is evidence of enhanced carbon storage within the Panama Basin as compared to the rest of the EEP during the LGM, I measured B/Ca ratios in benthic foraminifera to reconstruct bottom water [CO_3^{2-}] from a suite of cores across the EEP both within *and* outside

the Panama Basin. These records, specifically 17JC and MV1014-01-8JC (hereafter 8JC), were compared with previously generated aU, ^{232}Th, and xsBa proxy records from Loveley et al. (2017) and Marcantonio et al. (2020) to assess the possible influence of Fe fertilization on EEP carbon storage. If increased export production due to enhanced dust deposition is the controlling mechanism on regional carbon storage, then the [CO_3^{2-}] records should inversely covary (decreased [CO_3^{2-}] with increasing ^{232}Th/xsBa) with the ^{232}Th and xsBa records across the last deglaciation. If increased export production is not the main driver of regional carbon storage, and instead overall poor ventilation of source waters is the controlling mechanism, then the [CO_3^{2-}] should inversely covary with the previously generated aU records (decreasing [CO_3^{2-}] with increasing aU).

The four records generated in this study were then compared to other bottom water [CO_3^{2-}] records from the EEP to gain a better understanding of how carbon storage varied in the region since the LGM. This study incorporates cores spanning shallow (~2 km) to mid-depths (~3 km) in order to determine depth limits on the glacial EEP carbon reservoir. This depth range will allow for further constraints to be placed on the possible carbon storage gradient in the EEP during the LGM as well. Combining cores from inside and outside the Panama Basin at similar depths will determine the influence the Panama Basin itself may have had on regional carbon storage. Finally, by creating high-resolution records across the last 25 kyr, this study will examine the temporal variability of the hypothesized carbon reservoir across the last deglaciation and through the Holocene.

Oceanographic Setting

The modern EEP is a source of CO_2 to the atmosphere driven, primarily by strong regional upwelling of CO_2 rich waters of the Equatorial Undercurrent (Takahashi et al., 2009;

Fiedler and Talley, 2006). Although this upwelling also brings nutrient rich waters to the surface, biological productivity is limited by low concentrations of the micronutrient Fe (Dugdale & Wilkerson, Martin et al., 1994). As a result, macronutrients such as nitrate and phosphate are not fully used and their concentrations remain high due to this Fe limitation (Robinson et al., 2009). This unused nutrient supply in conjunction with the Fe limitation has led the EEP to be one of the largest HNLC areas in the modern ocean. (Le Borgne et al., 2002). Furthermore, the EEP HNLC region constitutes a major site of modern efflux of CO_2 from surface waters to the atmosphere (Takahashi et al. 2002).

The Panama Basin is bound by a series of ridge systems and the South and Central American coasts. The Cocos Ridge (sill depth ~1.9 km, Figure 1) constrains the west side of the Basin while the south side is bound by the Carnegie Ridge (sill depth ~2.3 km, Figure 1). The hydrography of the EEP, like the rest of the tropical Pacific, is connected to and influenced by Southern Ocean-originating water masses at depth. The deep waters of the Panama Basin are sourced by a branch of the southeast Pacific basin abyssal circulation that originates in the Antarctic Circumpolar Current (Tsuchiya and Talley, 1988). Antarctic Upper Circumpolar Deep Water (UCDW; Figure 2) forms the deep waters in the region as it spreads north from the Peru Basin entering the Panama Basin at a depth of 2.9 km through a small gap (3 km) between the Carnegie ridge and the South American coast (Laird, 1971; Lonsdale, 1977). Additional UCDW flows north into the Panama Basin over a broad saddle in the middle of the Carnegie Ridge at a depth of ~2.3 km (Lonsdale and Malfait, 1974). As UCDW travels north it begins to slowly undergo vertical mixing, ultimately forming Pacific Deep Water (PDW; Figure 2) in the North Pacific. This deep northern-sourced water mass is the oldest water mass on Earth, characterized by high-nutrients and low oxygen as well as elevated CO_2 concentrations (Fiedler & Talley,

2006). This PDW then returns south and forms the mid-depth (~1 km - 2.3 km) waters of the Panama Basin (Fiedler and Talley, 2006).

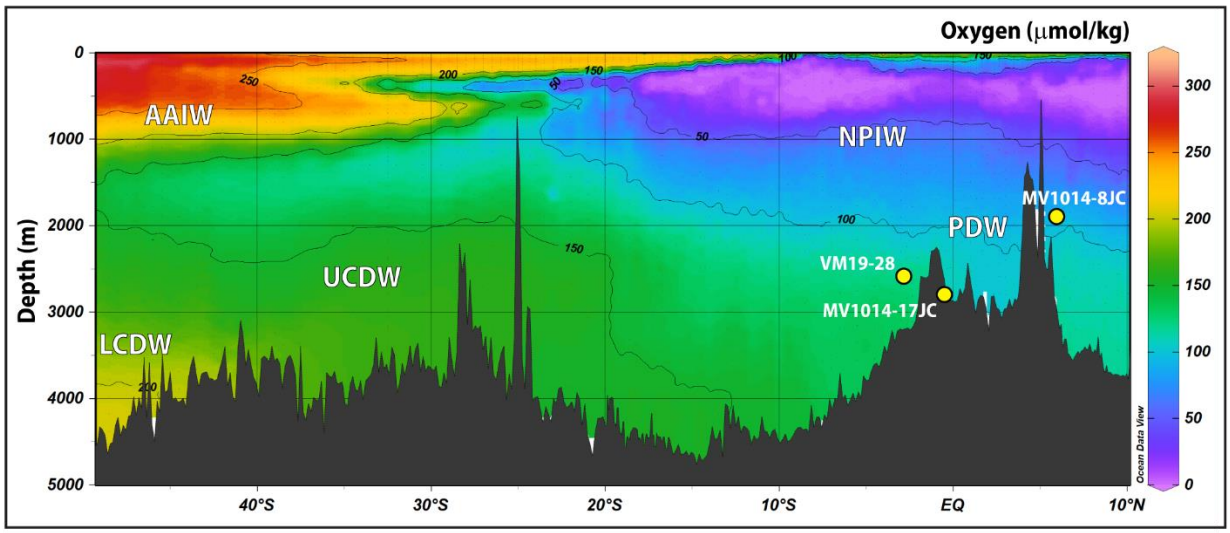

Figure 2: Eastern Pacific Hydrography. Modern Pacific dissolved oxygen concentration profile (color scale and contours) generated from the WOCE P19C transect (Schlitzer, 2017; Tsuchiya and Talley, 1993). Water masses are indicated: Lower Circumpolar Deep Water (LCDW), AAIW (Antarctic Intermediate Water), Upper Circumpolar Deep Water (UCDW), North Pacific Intermediate Water (NPIW), and Pacific Deep Water (PDW). Core locations from this study are indicated with yellow circles. Core TR163-22 not included due to its position far west outside of the transect.

Hydrographic profiles of modern seawater carbon system parameters are available for this region from the World Ocean Circulation Experiment (WOCE) P19C transect (Figure 3) (Talley, 2007). These seven vertical profiles from the P19C transect provide important insight into the region's modern water column chemistry. Modern Panama Basin hydrography exhibits signs of "biogeochemical aging" in the deeper parts of the basin as a result of the accumulation of respired carbon. These profiles show that modern regional export production is great enough to alter the inflowing source waters as they travel through the basin. This can be inferred by the increase of Alkalinity/DIC and the decrease of dissolved O_2 along the flow path of the deeper waters from south to north in the basin (Figure 3).

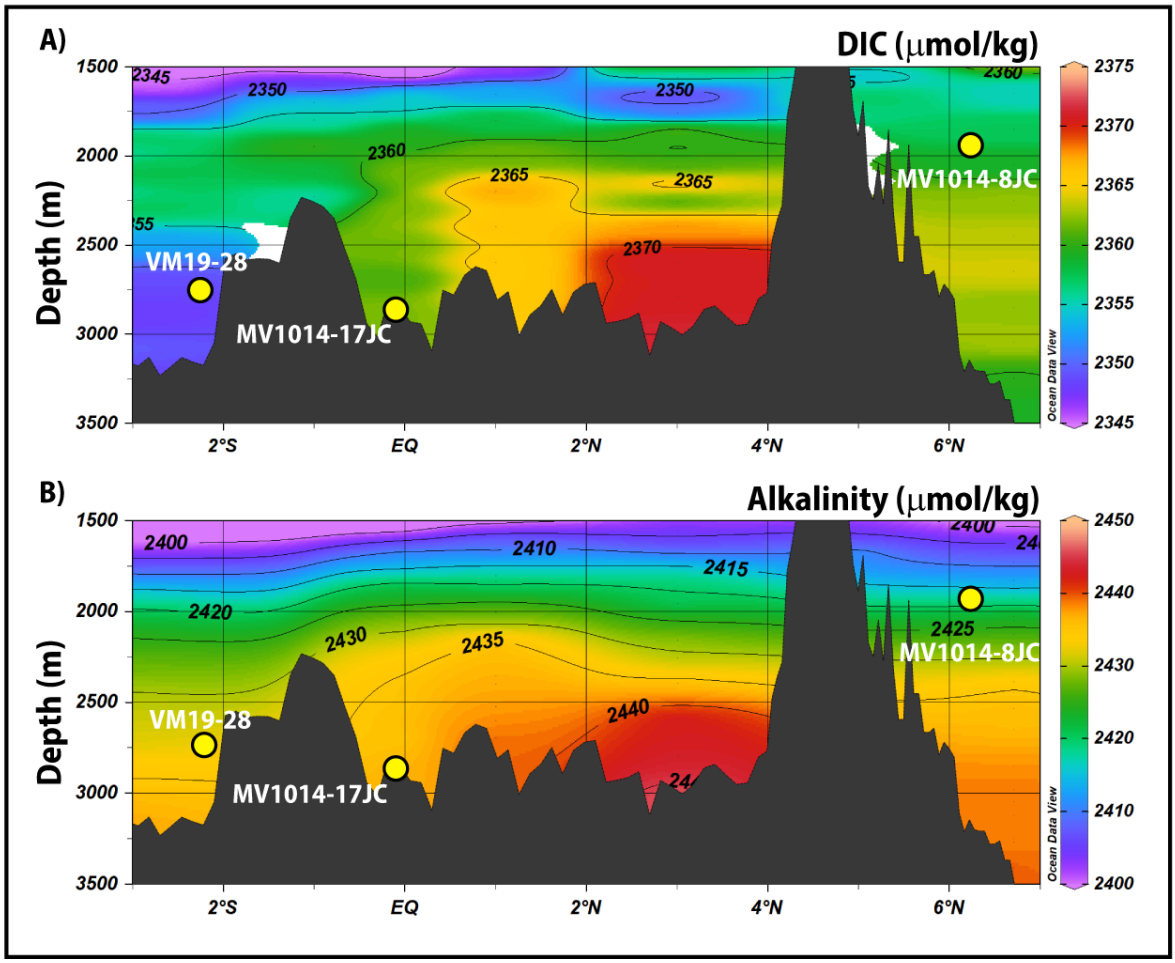

Figure 3: Panama Basin Hydrography. Hydrographic section data: **A)** Total Dissolved Inorganic Carbon (μmol/kg), and **B)** Total Alkalinity (μmol/kg) from the Panama Basin generated using the WOCE P19C transect (Tsuchiya and Talley, 1993). Core locations from this study are indicated with yellow circles. Core TR163-22 not included due to its position far west outside of the transect.

II. METHODS

Core Locations

I selected a suite of four cores spanning a depth range of 2 km to 2.9 km, with cores at similar depths from both inside and outside of the Panama Basin. This depth range allows for constraints to be placed on the vertical and horizontal extent of the deep carbon pool in the Panama Basin across the last 25 kyr. Core 8JC (6°14'N, 86°2'W) was collected from the Cocos Ridge, just outside of the Panama Basin, at 2 km water depth and represents the shallowest core used in this study (Figure 1). 17JC (0°10'S, 85°52'W) was retrieved from the Carnegie Ridge inside the Panama Basin at 2.9 km water depth and is used to represent the deepest conditions in the basin (Figure 1). Recovered from just outside the Panama Basin, VM19-28 (2°22'S, 84°39'W) lies at a similar depth (2.7 km water depth) to 17JC and provides a valuable opportunity to determine conditions at this depth south of the basin (Figure 1). Finally, TR163-22 (92°23.9'W, 0°30.9'N) was collected 200 km northwest of the Galapagos Islands at 2.8 km water depth and represents another deep location west of the basin for which to compare with 17JC (Figure 1). TR163-22 also lies the farthest distance west from the South American coast and is likely outside the influence of significant detrital input from the continental Americas. To summarize, three of the four cores, 8JC, VM19-28, and TR163-22, are from locations outside of the Panama Basin, while 17JC is from within the Panama Basin. I then combined my study sites with other cores from previously published studies in order to achieve a full range of depths and locations both within and outside of the Panama Basin (Figure 1). Core 17JC has the highest sedimentation rate and was used to generate sub-millennial scale records of rapid changes in the carbonate chemistry of the EEP in response to millennial scale climate events throughout the last

deglaciation. This is the first study to take this comprehensive of an approach with respect to depth related differences in carbon storage inside and outside of the Panama Basin.

Age Controls

The age model for 17JC is based on linear interpolation between ten radiocarbon dates analyzed on the planktic foraminifera *Neogloboquadrina dutertrei* from intervals within the top 500 cm of the core (Loveley et al., 2017). Sedimentation rates for 17JC range from 8 – 12 cm/kyr, corresponding to a sampling resolution of ~300 years. Importantly, 17JC has the highest sedimentation rate of any core recovered from the EEP, providing a unique opportunity to determine sub-millennial-scale climatic shifts and generate high-resolution records of the EEP deep water carbonate system. The age model for 8JC is based on linear interpolation between seven radiocarbon dates also analyzed on *N. dutertrei*, equating to a sedimentation rate that varies from 1.3 to 6.8 cm/kyr, giving a sampling resolution of ~300-900 years during the last deglaciation (Marcantonio et al., 2020). The age model for TR163-22 was created by linear interpolation between nine radiocarbon dates in the top 400 cm of the core by Lea et al. (2006). Although this core has a high sedimentation rate (~10 cm/kyr) for the region, only 30 sample intervals were available to use in this study, resulting in a lower deglacial age resolution. The age model for VM19-28 is based on linear interpolation between six radiocarbon dates published by Koutavas and Lynch-Stieglitz (2003). This core has a sedimentation rate of ~5 cm/kyr and enough sample intervals were available to generate a high-resolution record.

B/Ca Sample Preparation

Tests of the epifaunal benthic foraminifera *Cibicidoides wuellerstorfi (*also called *Planulina wuellerstorfi)* were picked from all available intervals spanning the last 25 kyr in the four cores from the >150 μm size fraction. This epifaunal species was chosen because infaunal

benthic foraminiferal species are subject to DIC changes in pore water due to the remineralization of organic material in the sediments (Yu and Elderfield, 2007). Furthermore, there are established equations to calculate carbonate system parameters from B/Ca ratios measured on *Cibicidoides wuellerstorfi* (Yu and Elderfield, 2007) (see section 2.6 below). 10-20 individuals totaling >250 µg (>150 µg in cases of low abundance) were carefully picked from each core interval, gently crushed to expose their inner chambers for cleaning, and homogenized. 112 intervals across all four cores yielded larger samples (> 500 µg) and were split into aliquots after homogenization to generate replicate analyses. Samples were then cleaned according to the protocol outlined by Schmidt et al. (2012) and modified to avoid boron contamination. The cleaning procedure included sonication in ultra-pure low boron Milli-Q water and methanol, treatments with hot oxidizing and reducing solutions to remove organic matter and metal oxide coatings, respectively, transfers to new boron-free acid leached vials, and a final leach with a weak, ultra-pure low boron 0.01% HNO_3 solution. All samples were cleaned in over-pressured flow hoods equipped with non-fiberglass HEPA filters to maintain trace metal clean conditions.

B/Ca Analysis

Samples were dissolved in 500 µL of ultra-pure low boron 2% HNO_3 and analyzed on a Thermo Scientific Element XR High Resolution Inductively Coupled Plasma Mass Spectrometer (HR-ICP-MS) at Old Dominion University's College of Sciences Major Instrument Cluster (COSMIC) lab. Sample vials were only opened immediately before analysis to avoid airborne boron "fall-in" contamination described by Rae et al. (2011). A series of trace and minor elements were analyzed and normalized to Ca including B, Mg, Fe, Al, and, Mn. Sample element/calcium ratios were determined from a linear calibration based on a series of four calibration standards of known Element/Calcium ratios analyzed between every set of six

samples during each run. Samples were also blank corrected based on sets of 2% HNO_3 blanks analyzed periodically throughout every run. 2% HNO_3 blanks were carefully monitored for any sources of boron contamination during the analysis process. Al/Ca, Fe/Ca, and Mn/Ca were used to monitor for any contaminants remaining after the cleaning procedure. Elevated ratios of Al/Ca values indicate the presence of aluminosilicate clays not removed during the cleaning process. High Fe/Ca and Mn/Ca indicate the presence of oxide coatings not removed during the reductive cleaning step. Samples with ratios of >100 μmol/mol for Al/Ca, Mn/Ca, or Fe/Ca were rejected due to potential contamination. Elevated manganese and iron values were expected during analysis due high levels of hydrothermal activity in this region (Lund et al., 2016). Repeated analysis of three consistency standards during each run were used to determine the analytical precision for each series of measurements. Reproducibility of values were based on duplicate analysis of samples split from within the same core interval when enough material was available.

Replicate and Analytical error

A total of 323 measurements (replicates included) were conducted for this study. Nineteen analyses were excluded based on either elevated cleaning indicators or low sample recovery weight: 10 were removed due to elevated Fe/Ca and Al/Ca (>100 μmol/mol) and 9 were removed due to low sample recovery weight (<10 μg) after cleaning. After removing these data, the final total number of accepted analyses in the study was 304. The B/Ca ratios across the cores ranged from 147.8 μmol/mol to 187.4 μmol/mol with an average of 172.3 μmol/mol. Recurrent analysis of three matrix-matched consistency standards with B/Ca ratios of 100 μmol/mol, 146 μmol/mol, and 201 μmol/mol yielded an analytical precision of ± 0.91%. It was determined that the 100 μmol/mol standard would not be included in the final calculations due to the higher range of measured B/Ca values measured in my samples. The calculated analytical

precision based on the 146 µmol/mol and 201 µmol/mol standards was 0.58 % or ± 1.00 µmol/mol for B/Ca based on an average analyzed B/Ca ratio of 172.3 µmol/mol. The B/Ca differences between replicates ranged from 0.6 µmol/mol (0.33%) to 12.7 µmol/mol (7.34%) with an average of 5.6 µmol/mol (3.37 %). The combined replicate and analytical RSDs ($\sqrt{RSD_A^2 + RSD_B^2}$) yielded an average standard error of ± 5.8 µmol/mol and an RSD of ± 3.4 %.

B/Ca based [CO_3^{2-}] calculations

The B/Ca ratios in the calcite tests of *C. wuellerstorfi* have been experimentally shown by Yu and Elderfield. (2007) to relate linearly to $\Delta[CO_3^{2-}]$ based on a global compilation of core top measurements. *C. wuellerstorfi* B/Ca can be converted to $\Delta[CO_3^{2-}]$ using a species-specific calibration (equation 1) that has an estimated accuracy of ±10 µmol kg^{-1} in reconstructed records. The relationship between B/Ca and $\Delta[CO_3^{2-}]$ then allows for downcore $[CO_3^{2-}]_{in\ situ}$ to be reconstructed based on equation 2. Seawater $[CO_3^{2-}]_{sat}$ in the modern ocean was determined from $[CO_3^{2-}]_{in\ situ}/\Omega_{Calcite}$ values where $\Omega_{Calcite}$ is the saturation state of calcite at a given salinity, pressure, and temperature (Table 1). A constant value for $[CO_3^{2-}]_{sat}$ was assumed throughout each core due to the small variability of salinity, temperature, and pressure over the late Pleistocene in the deep Pacific (Allen et al., 2015).

(1) $\Delta[CO_3^{2-}] = (B/Ca - 177.1)/1.14$ (µmol/kg)

(2) $\Delta[CO_3^{2-}] = [CO_3^{2-}] - [CO_3^{2-}]_{sat}$ (µmol/kg)

Modern day $\Delta[CO_3^{2-}]$, $[CO_3^{2-}]_{sat}$, and $\Omega_{Calcite}$ values (Table 2) for each core location were determined using Ocean Data View's ocean calculator software package (Schlitzer, 2015). The hydrographic information needed to calculate the carbonate system components included pressure (dbar), temperature (°C), salinity (unitless), phosphate concentration (µmol/kg), silicate

concentration (µmol/kg), total alkalinity (µmol/kg), and total DIC (µmol/kg) (Table 1). Consistent with previous studies in the region, the equilibrium constants of Dickson and Millero (1987) and Mehrbach et al. (1973) were applied in the calculations. Modern $[CO_3^{2-}]_{sat}$ values of 60.98 µmol/kg, 75.11 µmol/kg, 71.13 µmol/kg, 74.45 µmol/kg were used for cores 8JC, 17JC, TR163-22, and VM1928, respectively, based on the closest available hydrographic stations from the WOCE P19C transect (Tsuchiya and Talley, 1998) (Table 2).

Core	Pressure (dbar)	Temperature (°C)	Salinity (unitless)	Phosphate (µmol/kg)	Silicate (µmol/kg)	Alkalinity (µmol/kg)	DIC (µmol/kg)
MV1014-02-17JC	2925	1.82	34.67	2.75	153	2437	2362
MV1014-01-8JC	2071	2.04	34.65	2.80	146	2425	2359
VM19-28	2730	1.61	34.68	2.64	147	2431	2349
TR163-22	2925	1.82	34.67	2.75	153	2437	2362

Table 1: EEP Hydrographic Properties. Modern bottom water hydrography for each core used in this study.

Core	Latitude	Longitude	Depth (km)	$[CO_3^{2-}]$ (µmol/kg)	Ω	$[CO_3^{2-}]_{sat}$ (µmol/kg)	$\Delta[CO_3^{2-}]$ (µmol/kg)	$[O_2]$ (µmol/kg)
MV1014-02-17JC	0º10’ S	85º52’ W	2.9	67.58	0.90	75.11	-7.51	109
MV1014-01-8JC	6º14’ N	86º2’ W	2.0	62.20	1.02	60.98	1.22	94
VM19-28	2º22’ S	84º39’ W	2.7	72.31	0.97	74.55	-1.48	122
TR163-22	0º30’N	92º23’ W	2.8	67.58	0.95	71.13	-3.55	110

Table 2: EEP Carbonate Chemistry EEP location and modern bottom water carbonate chemistry for each core used in this study.

III. RESULTS

B/Ca results

The only core in my study from inside the Panama Basin (17JC: Figure 4, yellow line) exhibited the largest change in B/Ca across the last deglaciation. Starting before Heinrich Stadial 2 (HS2) at 26 kyr, B/Ca ratios decreased from 167 μmol/mol to 153 μmol/mol near the beginning of HS2. Ratios remained low during HS2, but then dropped to the lowest recorded measurement of 147 μmol/mol at approximately 20 kyr. The overall LGM (18 kyr - 23 kyr) B/Ca average of 157 μmol/mol for 17JC was the lowest glacial average out of the four records in my study. Following this glacial low, B/Ca ratios increased until the onset of HS1 when they dropped by 9 μmol/mol to a deglacial low of 153 μmol/mol. Towards the end of HS1, B/Ca ratios began to recover and increased consistently across the Bølling–Allerød (BA), ultimately reaching a ratio of 176 μmol/mol. Following the start of the Younger Dryas (YD), ratios rapidly decreased from the previous peak to a low of 160 μmol/mol. In a similar trend to HS1, ratios quickly increased after this low during the YD and reached a high of 180 μmol/mol near the start of the Holocene. Throughout the mid-Holocene ratios exhibited two distinct maximums at ~5.4 kyr and ~7.5 kyr with B/Ca ratios of 184 μmol/mol and 180 μmol/mol, respectively. The late-Holocene was characterized by an overall decrease in B/Ca to near modern ratios at the core-top (see Results section 3.2). The average Holocene (0-11.7 kyr) B/Ca for 17JC of 174 μmol/mol was 17 μmol/mol higher than the LGM average, the largest LGM-Holocene difference of the four B/Ca records created in this study.

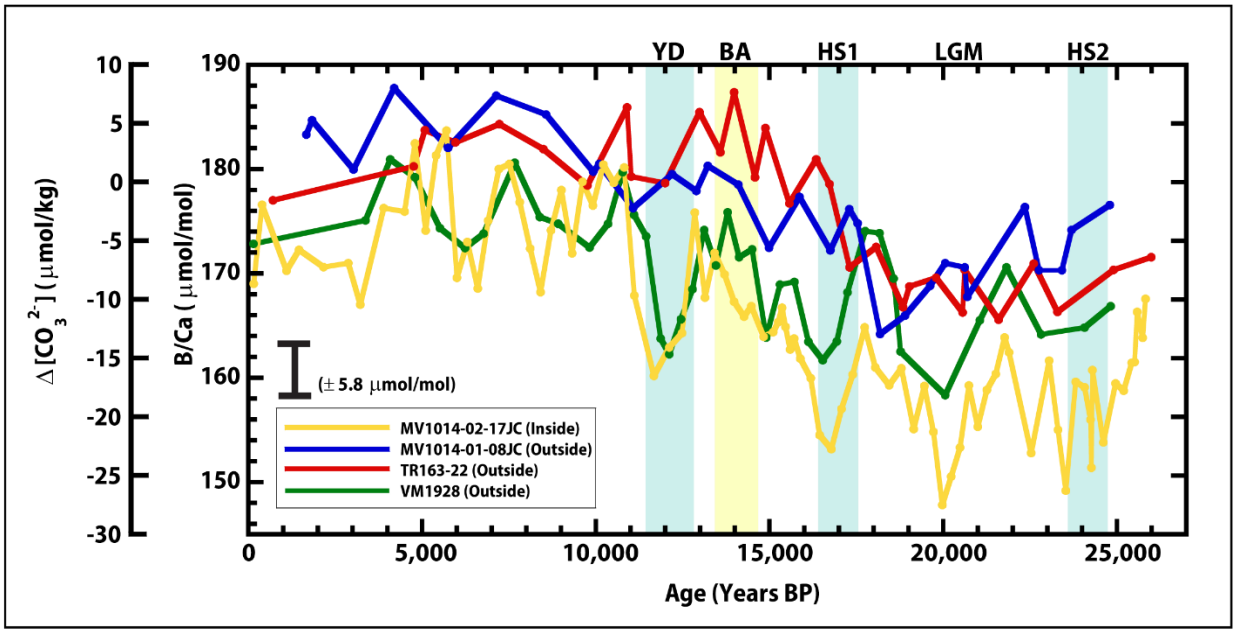

Figure 4: EEP B/Ca-Δ[CO_3^{2-}] Reconstructions. *C. wuellerstorfi* B/Ca records from the last 25 kyr for the four cores used in this study. B/Ca was converted to seawater Δ[CO_3^{2-}] using the original calibration of Yu and Elderfield (2007). Vertical Error bar represents ± 3.37 % (combined analytical and replicate variation RSD; see methods section 2.5 for details).

Results from core VM19-28 (Figure 4, green line) from just south of the Panama Basin exhibited broadly similar patterns to those seen in the 17JC record. Ratios decreased slightly across HS2 and then increased to a glacial maximum of 171 µmol/mol. This was followed by a decrease to the lowest glacial ratio of 158 µmol/mol at approximately 20 kyr. B/Ca ratios increased throughout the remainder of the LGM until the start of HS1. From an early HS1 high of 174 µmol/mol, ratios decreased by 12 µmol/mol to a low of 162 µmol/mol at ~16.5 kyr. Following the end of HS1, B/Ca ratios rebounded and then experienced a slight reduction before the onset of the BA. Throughout the BA, B/Ca ratios increased until ~13 kyr, when a decrease marked the beginning of the YD. Ratios decreased from 174 µmol/mol to a low of 162 µmol/mol during the middle of the YD. Following this YD decrease, B/Ca ratios rapidly increased to an

early Holocene high of 180 μmol/mol. The mid-Holocene showed two distinct peaks in B/Ca at 7.6 kyr and 4 kyr with measurements of 181 μmol/mol each time. During the late-Holocene B/Ca ratios decreased towards modern day ratios with a core-top measurement of 173 μmol/mol. The average Holocene B/Ca measurement for VM19-28 was 176 μmol/mol compared to its LGM average of 165 μmol/mol. The overall LGM-Holocene difference of -9 μmol/mol was the smallest difference seen in the four constructed records.

Core 8JC (Figure 4, blue line) from the shallowest depth (2 km) outside the Panama Basin to the north showed the second greatest difference between Holocene and LGM average B/Ca ratios. During HS2, ratios decreased slightly before rebounding to an LGM maximum of 176 μmol/mol. From this maximum, B/Ca ratios decreased through the remainder of the LGM and showed the lowest ratios of 164 μmol/mol at approximately 18.2 kyr. Following this glacial low, B/Ca ratios rapidly increased to 176 μmol/mol at the beginning of HS1 and remained relatively constant until a slight decrease to 173 μmol/mol before the beginning of the BA. Throughout the BA, B/Ca ratios consistently increased to a maximum of 180 μmol/mol just prior to the onset of the YD. During the YD B/Ca ratios decreased slightly, but then began to increase to an early-Holocene ratio of 181 μmol/mol. During the mid-to-late Holocene ratios remained relatively stable with an average of 182 μmol/mol. The core-top age of 8JC was 1.7 kyr and did not accurately reflect modern conditions at the core site. The Holocene average of 182 μmol/mol was the highest Holocene average of the four constructed records. The -13 μmol/mol difference between this Holocene average and the LGM average of 169 μmol/mol was the second largest of the four records. This difference was also the largest of the cores outside the Panama Basin.

Finally, westernmost core TR163-22 (Figure 4, red line) from outside of the Panama Basin showed the least amount of millennial-scale variability of my four records. Ratios

decreased slightly across HS2 and the LGM, reaching a minimum glacial B/Ca ratio of 167 μmol/mol. This was followed by a consistent increase across HS1 to a maximum of 184 μmol/mol just before the start of the BA. During the BA, a maximum B/Ca ratio of 187 μmol/mol was recorded. There were then a series of low B/Ca periods through the end of the BA and YD periods before an increase to 186 μmol/mol during the early-Holocene. Following this increase, ratios decreased and plateaued to near the Holocene average of 182 μmol/mol. When compared with the LGM average of 169 μmol/mol, TR163-22 had an LGM-Holocene difference of -12 μmol/mol, the second largest difference for the cores from outside of the Panama Basin.

Reconstructed [CO_3^{2-}] Records

The combined B/Ca-Δ[CO_3^{2-}] (methods section 2.6, equation 1) and modern [CO_3^{2-}]$_{sat}$ (methods section 2.6, equation 2) resulted in a [CO_3^{2-}] range from 49.4 μmol/kg to 84.1 μmol/kg with an average value of 67.2 μmol/kg across the four records (Figure 5). The pooled RSD on the B/Ca measurements of ± 3.37% equated to a standard error of ± 2.26 μmol/kg which was applied to each [CO_3^{2-}] record. Two of the four cores (17JC and VM19-28) had core top ages that allowed for comparison of reconstructed [CO_3^{2-}] to modern [CO_3^{2-}]$_{in\ situ}$. The modern [CO_3^{2-}] for 17JC is 67.58 μmol/kg compared to the reconstructed value of 69.67 μmol/kg, while VM19-28 has a modern [CO_3^{2-}] of 72.31 μmol/kg compared to a reconstructed value of 71.32 μmol/kg (Figure 5). The closeness of the reconstructed and modern empirical values provided strong confidence in the B/Ca proxy to accurately reconstruct bottom water conditions. The two other cores, which had significantly older core tops, had higher calculated core top [CO_3^{2-}] when compared with modern values at each site. These elevated values were likely due to increased [CO_3^{2-}] during the middle-late Holocene at the core sites.

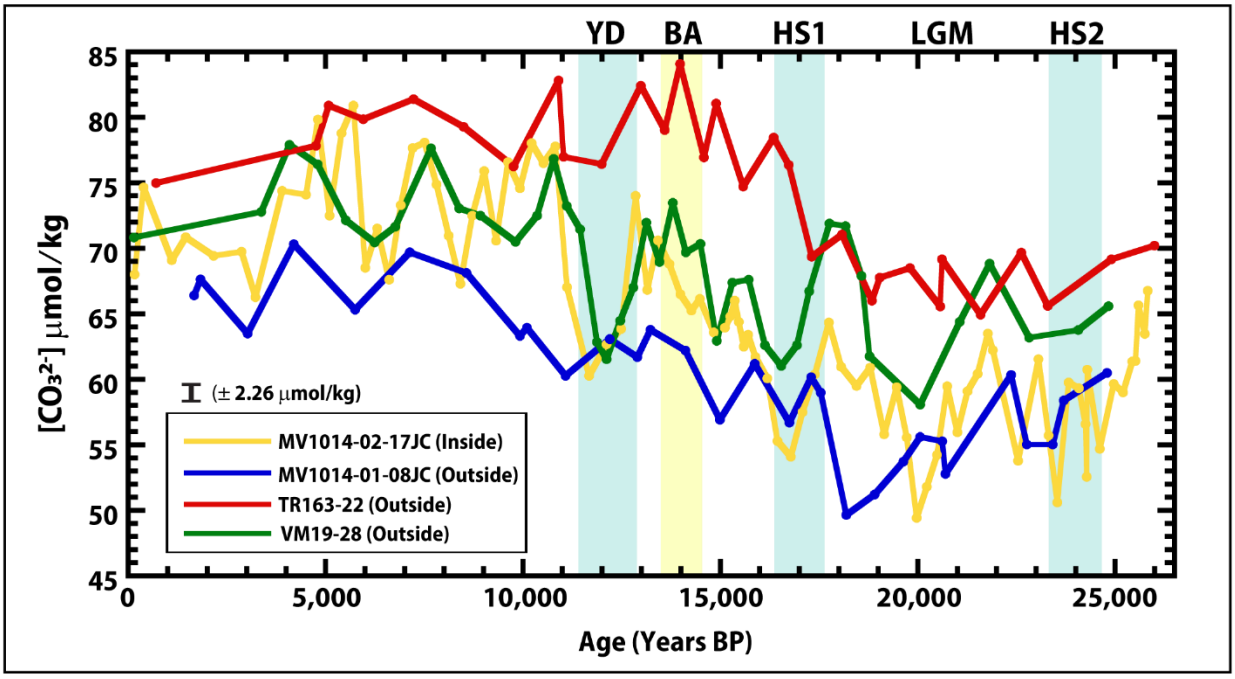

Figure 5: EEP [CO_3^{2-}] Records. [CO_3^{2-}] derived from B/Ca-Δ[CO_3^{2-}] (see methods section 2.6) from the last 25 kyr for the four cores in this study. Vertical Error bar represents ± 3.37 % (combined analytical and replicate variation RSD; see methods section 2.5 for details).

A depth profile of Holocene [CO_3^{2-}] was created from the average [CO_3^{2-}] data between 0 and 11.7 kyr for each core (Figure 6). Though the overall [CO_3^{2-}] was higher during the Holocene compared with modern EEP values, the profile closely reflected the structure of the modern EEP [CO_3^{2-}] distribution with depth. The exception to this was the Holocene average for the westernmost core TR163-22, which had a higher [CO_3^{2-}] when compared to the other cores at similar depths. Furthermore, every record displayed lower average [CO_3^{2-}] during the LGM than during the Holocene. The average glacial [CO_3^{2-}] outside the Panama Basin was lower than the Holocene average by -12 µmol/kg, -11 µmol/kg and, -8 µmol/kg at cores 8JC, TR163-22, and VM1928, respectively. The largest LGM-Holocene difference was -16 µmol/kg, recorded at 17JC *inside* the Panama Basin. The records both inside and outside the Basin showed their lowest overall values during the glacial period. The [CO_3^{2-}] values began to rise during the

deglaciation in all cores at approximately 19.5 kyr (Figure 5). Due to the variability in each record and the combined uncertainty of the age models and B/Ca-$\Delta[CO_3^{2-}]$ proxy, it was not feasible to assign a more precise timing for the initial shift following the glacial minimum.

Two of the cores located outside the basin (8JC and TR163-22) showed a gradual increase in $[CO_3^{2-}]$ through the deglaciation into the early Holocene and then decreased towards modern values (Figure 5). The two other records (17JC and VM19-28) showed an overall deglacial increase with two periods of noted decrease in $[CO_3^{2-}]$ during HS1 (17.5 kyr -16.5 kyr) and the YD (12.9 kyr -11.7 kyr). During HS1, $[CO_3^{2-}]$ decreased from 72 µmol/kg to 61 µmol/kg in VM1928 and from 64 µmol/kg to 55 µmol/kg in 17JC. A comparable change in $[CO_3^{2-}]$ was recorded during the YD from 72 µmol/kg to 62 µmol/kg in VM1928 and from 74 µmol/kg to 60 µmol/kg in 17JC. The four records exhibited a slight early Holocene maximum in $[CO_3^{2-}]$ and then an overall decrease throughout the Holocene to near modern values. During the middle-late Holocene, 17JC and VM1928 displayed a series of roughly covarying minor oscillations, while TR163-22 and 8JC maintained a more stable plateau in $[CO_3^{2-}]$ (Figure 5).

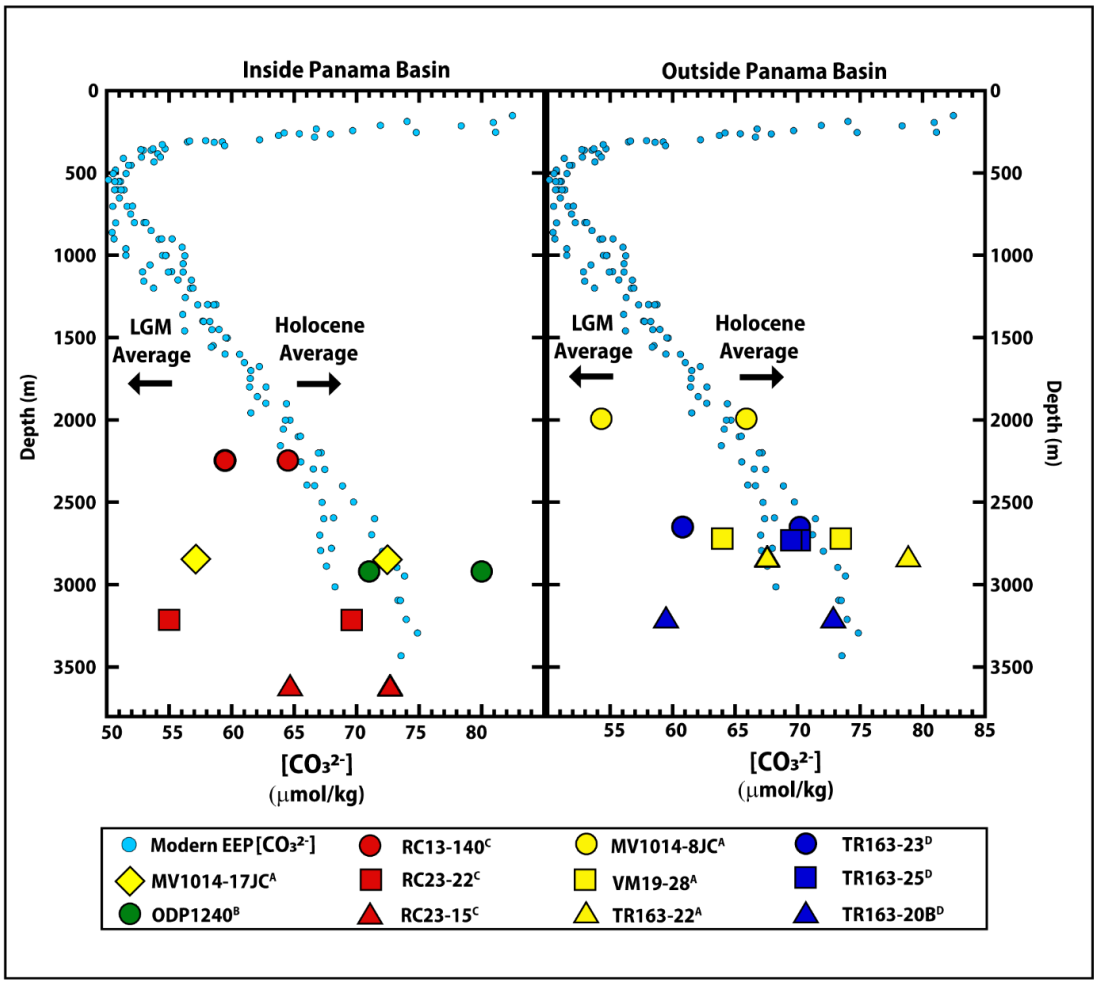

Figure 6: EEP Carbon Storage Comparison. Depth profiles of modern $[CO_3^{2-}]$ (blue dots) from the WOCE P19C transect (Tsuchiya and Talley, 1993) plotted with benthic foraminiferal B/Ca derived $[CO_3^{2-}]$ averages for the Holocene (0–11.7 kyr) and LGM (18.1 kyr–23.0 kyr) from the EEP. **A**, Averages from this study (yellow) and previously published records including: **B**, De la Fuente et al., 2017 (green), **C**, Doss and Marchitto, 2013 (red), and **D**, Umling and Thunell, 2018 (blue).

IV. DISCUSSION

Throughout the modern deep ocean, including the EEP, patterns of [CO_3^{2-}] are largely influenced locally by the degradation of organic matter and regionally by changes in source waters (Broecker and Peng, 1982). The generation of CO_2 from the respiration of marine organic matter has the effect of increasing DIC and decreasing [CO_3^{2-}] by lowering the pH of a water mass (Yu and Elderfield, 2007). As a result, modern deep water [CO_3^{2-}] decreases proportionally as organic matter is respired and the water mass ages (Yu and Elderfield, 2007). This relationship is the cause for the very low [CO_3^{2-}] in older Pacific deep waters when compared to equivalent depths in younger Atlantic waters (Yu and Elderfield, 2007). Although the mechanism that controls respired CO_2 storage in the deep Pacific during the LGM remains unclear, reconstructions of [CO_3^{2-}] have provided evidence for increased respired CO_2 storage (Doss and Marchitto, 2013; De La Fuente et al., 2017; Umling and Thunell, 2018, Yu et al., 2013, Allen et al., 2015; Allen et al., 2020).

LGM – Holocene [CO_3^{2-}] differences in the EEP

My new results from cores at depths of 2.9 km (17JC) inside the Panama Basin, and 2.8 km (TR163-22), 2.7 km (VM19-28), and 2.0 km outside the Panama Basin (8JC) all show that benthic foraminiferal B/Ca ratios were lower during the LGM (Figure 4), indicating lower [CO_3^{2-}]. When comparing the 17JC (2.9 km) [CO_3^{2-}] reconstruction from inside the Panama Basin with the [CO_3^{2-}] records from outside the basin at similar depths (VM19-28 (2.7 km) and TR163-22 (2.8 km)), it is clear that 17JC has the largest LGM-Holocene [CO_3^{2-}] difference of -16 µmol/kg (Figure 6, yellow diamond). TR163-22 has a difference of -11 µmol/kg (Figure 6, yellow triangle) while VM19-28 has the smallest of -8 µmol/kg (Figure 6, yellow square). These LGM [CO_3^{2-}] differences suggest that waters at the same depth just south and west of the

Panama Basin may have contained less respired CO_2 as compared to the waters inside the basin during the LGM.

De La Fuente et al. (2017) generated a benthic foraminiferal B/Ca based [CO_3^{2-}] reconstruction from a core at a depth (2.9 km) inside the Panama Basin near 17JC and also found lower glacial [CO_3^{2-}] (Figure 6, green circle). Their LGM – Holocene [CO_3^{2-}] difference was -11 µmol/kg, although their overall calculated [CO_3^{2-}] for both the LGM and the Holocene were higher than those in 17JC and also higher than the modern concentration. Another record from a core inside the Panama Basin reported the largest LGM-Holocene [CO_3^{2-}] difference of -15 µmol/kg at 3.2 km (Doss and Marchitto (2013) (Figure 6, red square). At a similar depth outside the basin (3.2 km) Umling and Thunell (2018) found a difference of -13 µmol/kg from the LGM to Holocene (Figure 6, blue triangle). This series of comparisons suggest that during the LGM, waters inside the Panama Basin had overall lower [CO_3^{2-}], suggesting the storage of a greater amount of respired CO_2 relative to waters at equivalent depths outside the basin. The increased carbon storage inside the Panama Basin and in the greater EEP during the LGM provides further evidence that the deep Pacific was indeed enriched in respired CO_2 during the LGM and contributed to the lower pCO_2 at that time.

Vertical differences in LGM [CO_3^{2-}] in the EEP

In addition to the geographic influence of the Panama Basin on deep water carbon storage, my new records suggest differences in the vertical distribution of respired CO_2 storage in the EEP during the LGM. In addition to 17JC at 2.9 km, Doss and Marchitto (2013) reconstructed [CO_3^{2-}] records at three depths inside the basin (2.2 km, 3.2 km and 3.6 km) and showed lower LGM [CO_3^{2-}] values in all three records. In their deepest core at 3.6 km they record an LGM-Holocene difference of -8 µmol/kg (Figure 6, red triangle). Moving upward the

values decrease to the largest LGM-Holocene difference of -15 µmol/kg at 3.2 km (Figure 6, red square). 17JC at 2.9 km shows the largest LGM-Holocene difference inside the basin of -16 µmol/kg. Finally, the shallowest core from Doss and Marchitto (2013) at 2.2 km shows the smallest LGM-Holocene difference of -5 µmol/kg (Figure 6, red circle). This profile suggests that there was a vertical gradient in the storage of respired CO_2 inside the basin with an increase from 2.2 km to 3.2 km and then a subsequent decrease below 3.2 km (Figure 6). The vertical difference of -11 µmol/kg between waters at 2.2 km and 2.9 km demonstrates that inside the basin, respired CO_2 storage increased with depth reaching a maximum [CO_3^{2-}] difference near 2.9 km.

The cores from this study outside the Panama Basin also show lower glacial B/Ca ratios indicating lower [CO_3^{2-}]. Umling and Thunell (2018) recorded lower glacial [CO_3^{2-}] from several cores outside the basin at 3.2 km, 2.8 km, and 2.7 km (Figure 6, blue symbols). They record their largest LGM-Holocene difference of -13 µmol/kg at 3.2 km depth (Figure 6, blue triangle). Moving upward, from this study, TR163-22 shows a difference of -11 µmol/kg at 2.8 km and VM19-28 shows a difference of -8 µmol/kg at 2.7 km (Figure 6, yellow triangle and Figure 6, yellow square). From two cores at nearly equivalent depths, Umling and Thunell (2018) report a difference of -0.7 µmol/kg and -9 µmol/kg at 2.7 km and 2.6 km, respectively (Figure 6, blue triangle and Figure 6, blue square). The shallowest core is my new record from 8JC at 2.0 km and it shows an LGM-Holocene difference of -12 µmol/kg (Figure 6, yellow circle). This profile constructed from outside the basin suggests that there was not a vertical gradient in respired CO_2 storage outside the basin. The difference between 8JC at 2.0 km and TR163-20B at 3.2 km is -1 µmol/kg, with no major variations occurring between these two depths. When compared with the magnitude of the -11 µmol/kg difference recorded from inside the basin, a vertical gradient in

respired CO_2 storage likely did not exist outside the basin. This provides further evidence that the waters inside the Panama Basin stored a greater amount of respired CO_2 relative to the rest of the EEP, and likely acted as an important carbon reservoir during the LGM.

Millennial-scale Deglacial [CO_3^{2-}] changes inside the Panama Basin

Due to the lower resolution of all the previously generated [CO_3^{2-}] records, millennial scale changes in respired CO_2 storage in the EEP were difficult to interpret and as a result, only differences on glacial-interglacial timescales were determined. The new high-resolution record from 17JC allows for the unique opportunity to go beyond glacial-interglacial changes and discern millennial-scale variations in respired CO_2 storage inside the Panama Basin across the last deglaciation (Figure 7). Several large deglacial shifts can be noted in 17JC's [CO_3^{2-}] record that occur during NH cold periods. During the last glacial period, [CO_3^{2-}] values decrease across HS2 to values similar to those during the LGM (Figure 7). During the last deglaciation, two NH cold periods elicit a similar response in the [CO_3^{2-}] record. During HS1 (17.5 kyr – 16.5 kyr) values decrease compared to the background deglacial trend. Following this drop, values steadily increase across the BA (14.5 kyr -13.5 kyr), a period of warming in the NH. The [CO_3^{2-}] values again decrease at the start of the YD (12.9-11.5) (Figure 7). These two decreases in [CO_3^{2-}] during the last deglaciation are large deviations from the overall deglacial increase from 20 kyr to 11 kyr. These periods of lowered [CO_3^{2-}] suggest greater storage of respired CO_2, possibly indicating the EEP acted as a sink for atmospheric pCO_2 during these cold climate intervals.

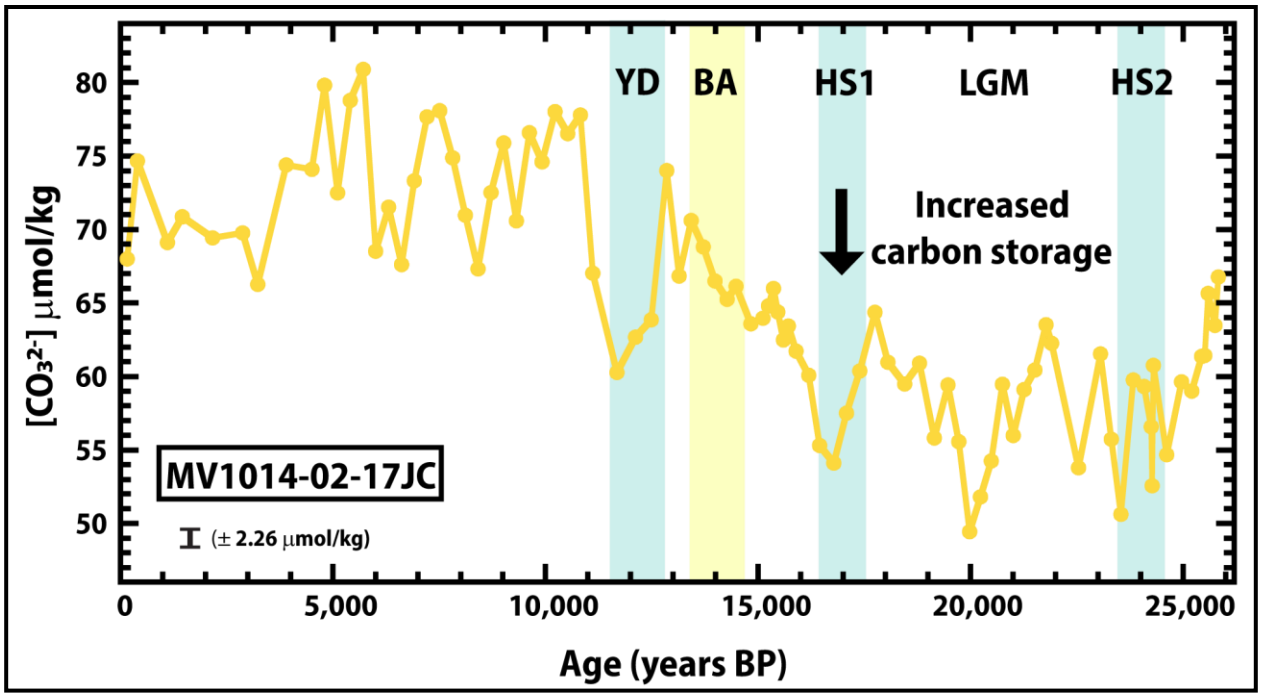

Figure 7: EEP Millennial-Scale [CO_3^{2-}] Record. B/Ca-[CO_3^{2-}] record for 17JC across the last deglaciation. NH cold periods are indicated with a blue bar: HS2, HS1, and YD. NH warm periods are indicated with a yellow bar: BA. (Error bar represents the combined analytical standard error and replicate standard error for each measurement of ± 2.26 µmol/kg)

Mechanisms for [CO_3^{2-}] changes in the EEP across the last deglaciation

Bottom water oxygenation

As respired [CO_2] increases in a water mass, due to either poor ventilation of the source waters or increased respiration of exported surface organic matter, dissolved oxygen content decreases (McManus et al., 2005). In order to determine if the changes in the [CO_3^{2-}] records from this study are the result of poor ventilation of source waters in the glacial Pacific or increased local export production, a separate bottom water oxygenation proxy is necessary. Authigenic Uranium (aU) concentrations have been successfully used in previous studies to evaluate the oxygen content of bottom waters throughout the Pacific (Jaccard et al., 2009; Jaccard et al., 2016; Loveley et al.,2017; Bradtmiller et al.,2010, Marcantonio et al., 2020).

There are two major controls on bottom water oxygenation that influence the concentration of aU in sediment: the rain of reducible organic material from the surface ocean, which consumes oxygen as it is respired thus increasing aU (Francois et al., 1993), and the oxygen content of the source water bathing the ocean floor, which is primarily influenced by ventilation (Thomson et al., 1990). If a deep-water mass becomes isolated from interaction with surface waters (i.e. poor ventilation) it will accumulate nutrients in addition to an increase in respired CO_2 concentration and a decrease in dissolved oxygen content due to respiration (therefore increasing aU concentrations) (Thomson et al., 1990). This poor ventilation can influence bottom water oxygen content, and therefore increase aU concentrations, independent of any export production changes.

The previously referenced studies from throughout the Pacific inferred greater respired CO_2 storage based on higher aU concentrations (lower oxygen) in deep waters of the Pacific during the LGM. The spatial and temporal consistency of these aU records lends support to the idea that the entire Pacific was influenced by a poorly ventilated deep water mass enriched in respired CO_2 as opposed to each record being influenced by increases in regional export production alone. Here, the new [CO_3^{2-}] records are compared with the previously published aU records for 17JC (Loveley et al., 2017) and 8JC (Marcantonio et al., 2020) in order to determine if either reduced water mass ventilation or increased export production had a controlling influence on respired carbon storage in the EEP (Figure 8 and Figure 9). Marcantonio et al. (2020) noted that the aU records for both cores are very similar despite the depth difference between 17JC and 8JC (2.8 km and 2 km, respectively) as well as the geographic differences (17JC inside the Panama Basin along the equator and 8JC farther north outside the basin). The aU concentrations reconstructed from both cores have ranges from 8-12 ppm with the highest aU

concentrations (and hence lowest bottom water [O_2]) occurring between 19 and 20 kyr during the LGM (Figure 8D and Figure 9D).

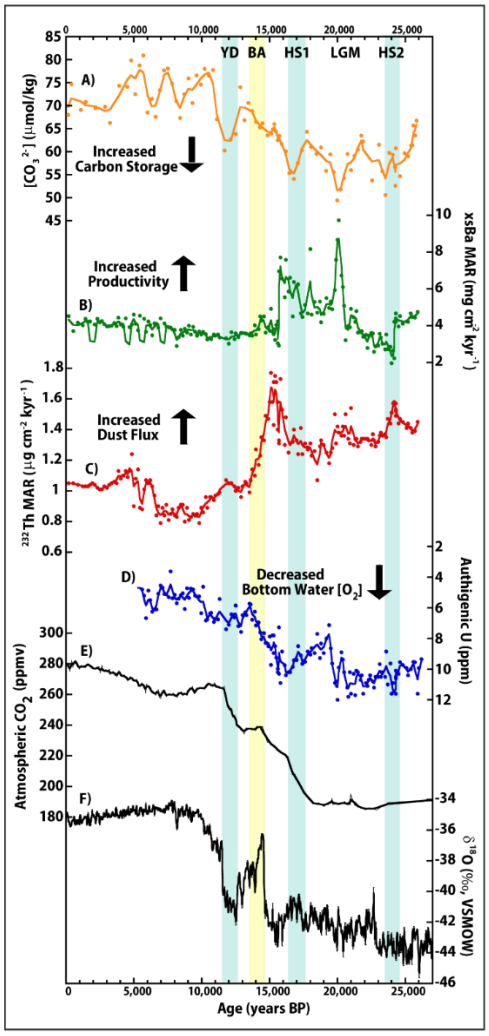

Figure 8: 17JC Intra-Core Proxy Comparison. Proxy data from core MV1014-02-17JC: **A**, [CO_3^{2-}] (orange line), a proxy for respired CO_2 storage, (this study), **B** ^{230}Th-normalized xsBa flux (green line), a proxy for export production (Loveley et al., 2017), **C**) ^{230}Th-normalized ^{232}Th flux (red line), a proxy for dust flux (Loveley et al., 2017), **D**) Authigenic Uranium (blue line), a proxy for bottom-water oxygenation (Loveley et al., 2017), **E**) Atmospheric CO_2 record from Antarctic ice cores (Bereiter et al., 2012) (grey line), **F**) NGRIP d^{18}O record (Johnson et al., 2004) (black line)

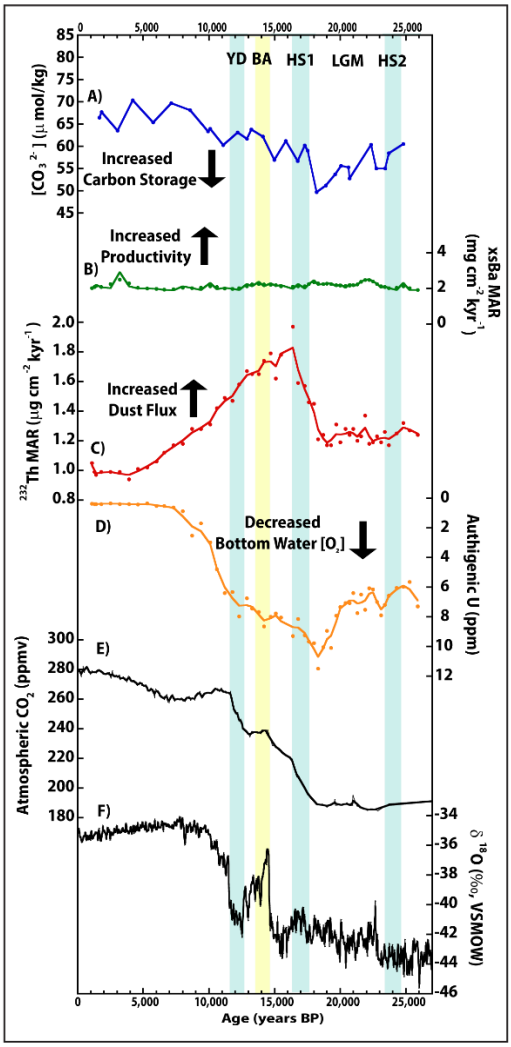

Figure 9: 8JC Intra-Core Proxy Comparison. Proxy data from core MV1014-01-8JC: **A**, $[CO_3^{2-}]$ (blue line), a proxy for respired CO_2 storage, (this study), **B** ^{230}Th-normalized xsBa flux (green line), a proxy for export production (Marcantonio et al., 2019), **C**) ^{230}Th-normalized ^{232}Th flux (red line), a proxy for dust flux (Marcantonio et al., 2019), **D**) Authigenic Uranium (orange line), a proxy for bottom-water oxygenation (Marcantonio et al., 2019), **E**) Atmospheric CO_2 record from Antarctic ice cores (Bereiter et al., 2012) (grey line), **F**) NGRIP $d^{18}O$ record (Johnson et al., 2004) (black line)

For both 17JC and 8JC, the reconstructed $[CO_3^{2-}]$ records resemble the aU records (Figure 8D and Figure 9D). In both cores, aU reaches its highest concentration (lowest bottom water oxygenation) during the LGM at the same point that $[CO_3^{2-}]$ values reach their lowest in

each core (highest concentration of respired CO_2). This indicates that the bottom waters bathing each core location were lowest in oxygen and highest in respired CO_2 at the same time during the LGM. While the overall relationship for the aU and [CO_3^{2-}] records for both cores follow the same long-term trends, there are millennial-scale variations in the record for 17JC not present in 8JC. This likely indicates that on longer timescales oxygen concentrations and respired CO_2 storage at the core locations for 8JC and 17JC are being influenced by the same mechanism. On shorter, millennial timescales, oxygen concentrations and respired CO_2 storage at the core location for 17JC are being influenced by a different mechanism independent of the long-term change seen in the waters at 8JC's core location. This in part supports the theory that a poorly ventilated deep Pacific water mass could have influenced the EEP as a whole and acted as a reservoir for CO_2 during the glacial period leading to lower atmospheric pCO_2. Additionally, based on the comparison of the 17JC records the influence of localized productivity cannot be overlooked as a large factor on changes in regional deep water respired CO_2 storage.

Dust Flux and surface water productivity in the EEP

Although the surface waters at site 17JC receive abundant nutrients due to upwelling, productivity in this region is limited today by the micronutrient Fe (Dugdale & Wilkerson, 1998; Martin et al., 1994). In two previous studies from 17JC and 8JC, deglacial ^{232}Th records were interpreted to reflect iron rich continentally derived dust fluxes to the core sites (Figure 8C and Figure 9C). Loveley et at. (2017) hypothesized that during NH cold periods, the ITCZ shifted as far south as the equator, thus increasing dust flux to the EEP. This increased dust flux relaxed the normal Fe limitation of the region and allowed for productivity to increase. Increased dust fluxes were recorded at both 17JC and 8JC across the last deglaciation (Figure 8C and Figure 9C).

When compared with the previously generated ^{232}Th flux record from Loveley et al. (2017) the [CO_3^{2-}] record from this study appears to have an inverse relationship (Figure 8A and 8C). Periods of lower [CO_3^{2-}] occur during times of increased ^{232}Th flux. This inverse relationship between increased dust flux and decreased bottom water [CO_3^{2-}] appears in 17JC during HS2, the LGM (~20 kyr), briefly during HS1, and briefly during the YD (Figure 8C). All four of these are NH cold stadials are associated with an overall increase in NH dust and a southward shift of the ITCZ near the equator (Loveley et al., 2017). It is theorized that the increase in dust flux during these cold periods associated with a southward displacement of ITCZ increased export production by relaxing the normal Fe limitation in the region. Therefore, in addition to the previously noted poorly ventilated Pacific deep-water influence, increased export production likely acted as a complementary mechanism increasing the amount of CO_2 stored in the waters bathing 17JC inside the Panama Basin.

Sea surface productivity recorded by xsBa in the EEP

Barite ($BaSO_4$) makes up the majority of the biogenically produced barium in the ocean, and in the modern ocean, barium enrichment occurs in sediments that underlie highly productive surface waters (Drymond et al 1992). By removing the continentally-derived aluminosilicate Ba from the total sedimentary Ba load, the excess Ba (xsBa) from barite produced authigenically (i.e., precipitated) can be estimated (McManus et al., 1998). As result, fluxes of xsBa have been used to determine changes in paleoproductivity in marine environments (Griffith and Payton, 2012).

Excess Ba records were previously published for cores 17JC (Loveley et al., 2017) and 8JC (Marcantonio et al., 2020) (Figure 8B and Figure 9B), allowing for evaluation of the relationship between paleoproductivity and [CO_3^{2-}] changes in the EEP. The xsBa records for

17JC and 8JC differ in both their average value and overall variability. The deglacial range of xsBa flux for 17JC (~2-10 μg cm^{-2}) is much larger than that of 8JC (~1.2-2.8 μg cm^{-2}). In addition, the overall average xsBa flux for 17JC (~4 μg cm^{-2}) is greater than that in 8JC (~2 μg cm^{-2}) (Figure 8B and Figure 9B).

When compared with their respective [CO_3^{2-}] records, the xsBa flux record in 17JC displays a distinct relationship, while the 8JC records show no such association (Figure 8A and Figure 9A). In 17JC, the two periods of highest xsBa flux (highest surface water productivity) coincide with the lowest [CO_3^{2-}] values (greatest respired CO_2 storage) during the LGM at ~20 kyr and across the deglaciation during HS1 (17.5 kyr – 16.5 kyr) (Figure 9B). This suggests that increased export production during these periods was great enough to modify carbon storage inside the Panama Basin. The fact that the 17JC [CO_3^{2-}] and xsBa flux records show similar trends while 8JC does not is likely due to the geographic position of the cores. 17JC is located within the heart of the eastern Pacific cold tongue that is characterized by strong upwelling (Loveley et al., 2017). Because the equatorial EEP is a HNLC region, productivity is very sensitive to aeolian Fe supply. As suggested in Loveley et al. (2017) a southward shift of the ITCZ to near the equator during Northern Hemisphere cold periods likely had a large impact on productivity at 17JC. On the other hand, 8JC is located farther north and outside the influence of the upwelling zone, so productivity at this location is not expected to be as sensitive to aeolian Fe supply (Marcantonio et al., 2020). Therefore, based on the relationship between xsBa and [CO_3^{2}] for 17JC, it is likely that changes in paleoproductivity had a significant impact on bottom water [CO_3^{2}].

It is interesting to note that there is little apparent relationship between dust flux and bottom water [CO_3^{2-}] in 8JC (Figure 9C). This too can be explained by the lack of a consistent

nutrient supply to the surface waters above the core. Even if Fe were being supplied by continentally derived dust, the lack of available macronutrients would mean that productivity would still be limited. It can be concluded, therefore, that the changes in bottom water oxygenation (as seen from the aU record) and [CO_3^{2-}] at 8JC are due to variability in water mass ventilation, and not export production. Whereas the [CO_3^{2-}] changes in 17JC, in addition to the impact of the previously noted poorly ventilated water mass, are significantly influenced by both changes in surface water productivity and carbon export.

V. CONCLUSIONS

The new benthic foraminiferal B/Ca-$\Delta[CO_3^{2-}]$ records presented in this study from within and outside the Panama Basin illustrate that during the LGM, carbonate ion concentrations were at their lowest levels over the last 25 kyr. This indicates that respired CO_2 storage increased in the EEP at depths from 2 km – 2.9 km at the same time that atmospheric CO_2 was at its lowest levels. The increased storage in this depth range supports the hypothesis presented by Sigman and Boyle (2000) that the deep Pacific acted as a respired CO_2 reservoir and aided in lowering atmospheric CO_2 during the last glacial period. The offset in the magnitude of the LGM-Holocene $[CO_3^{2-}]$ differences between the cores inside the basin (17JC) and outside the basin (8JC, VM19-28, and TR163-22) demonstrates that waters inside the basin stored a greater amount of respired CO_2 relative to waters at similar depths outside the basin. By including previously published $[CO_3^{2-}]$ records from a variety of depths from both inside and outside the Panama Basin, $[CO_3^{2-}]$ depth profiles show that during the LGM there was a vertical gradient in respired CO_2 storage inside the basin, increasing from 2.2 km to a maximum occurring near 2.9 km. Further, the depth profile created from cores outside the basin shows that respired CO_2 storage was generally homogeneous from 2 km to 3.2 km during the LGM. The sub-millennial scale $[CO_3^{2-}]$ record for 17JC indicated that respired CO_2 storage inside the Panama Basin underwent two large millennial scale increases (low $[CO_3^{2-}]$) during the last deglaciation during HS1 and the YD, both NH cold stadials.

The $[CO_3^{2-}]$ records for 17JC and 8JC were compared with previously generated xsBa, ^{232}Th, and aU records from Loveley et al. (2017) and Marcantonio et al. (2020). The $[CO_3^{2-}]$ record generated here for 8JC closely followed the aU record, while showing no relationship to the xsBa or ^{232}Th records. It can be concluded, therefore, that increased glacial CO_2 storage at

this core location was unrelated to export productivity and likely was a result of a Pacific-wide, poorly ventilated water mass rich in respired CO_2. The [CO_3^{2-}] record for 17JC also resembled the aU record indicating this core location was also influenced by a Pacific-wide, poorly ventilated water mass. However, unlike 8JC, the [CO_3^{2-}] record for 17JC displayed a relationship with previously generated ^{232}Th and xsBa records. Therefore, it can be concluded that in addition to the previously noted water mass influence, respired CO_2 storage at this core location was further enhanced by increased export production that was driven by dust derived iron fertilization. This enhanced storage due to increased productivity is likely the source for the difference between the magnitude of changes within and outside the Panama Basin. By sequestering carbon away from the atmosphere and surface ocean, deep waters in the Panama Basin and surrounding EEP likely played an important role in lowering glacial atmospheric CO_2. Further, as a result of several periods of enhanced surface productivity across the deglaciation, the efflux of CO_2 was likely dampened in the region, possibly slowing the deglacial increase in atmospheric CO_2 during HS1 and the YD.

REFERENCES

Allen, K. A., Sikes, E. L., Hönisch, B., Elmore, A. C., Guilderson, T. P., Rosenthal, Y., & Anderson, R. F. (2015). Southwest Pacific deep water carbonate chemistry linked to high southern latitude climate and atmospheric CO2 during the Last Glacial Termination. *Quaternary Science Reviews*, *122*, 180-191.

Allen, K. A., Sikes, E. L., Anderson, R. F., & Rosenthal, Y. (2020). Rapid loss of CO2 from the South Pacific Ocean during the last glacial termination. *Paleoceanography and Paleoclimatology*, *35*(2), e2019PA003766.

Barnes, C. E., & Cochran, J. K. (1990). Uranium removal in oceanic sediments and the oceanic U balance. *Earth and Planetary Science Letters*, *97*(1-2), 94-101.

Bradtmiller, L. I., Anderson, R. F., Sachs, J. P., & Fleisher, M. Q. (2010). A deeper respired carbon pool in the glacial equatorial Pacific Ocean. *Earth and Planetary Science Letters*, *299*(3-4), 417-425.

Bereiter, B., Lüthi, D., Siegrist, M., Schüpbach, S., Stocker, T. F., & Fischer, H. (2012). Mode change of millennial CO2 variability during the last glacial cycle associated with a bipolar marine carbon seesaw. *Proceedings of the National Academy of Sciences*, *109*(25), 9755-9760.

Broecker, W., & Barker, S. (2007). A 190‰ drop in atmosphere's Δ14C during the "Mystery Interval" (17.5 to 14.5 kyr). *Earth and Planetary Science Letters*, *256*(1-2), 90-99.

Broecker, W., Barker, S., Clark, E., Hajdas, I., Bonani, G., & Stott, L. (2004). Ventilation of the glacial deep Pacific Ocean. *Science*, *306*(5699), 1169-1172.

Broecker, W. S., & Peng, T. H. (1982). Tracers in the Sea.

Calvo, E., Pelejero, C., Pena, L. D., Cacho, I., & Logan, G. A. (2011). Eastern Equatorial Pacific productivity and related-CO2 changes since the last glacial period. *Proceedings of the National Academy of Sciences*, *108*(14), 5537-5541.

De La Fuente, M., Calvo, E., Skinner, L., Pelejero, C., Evans, D., Müller, W., ... & Cacho, I. (2017). The evolution of deep ocean chemistry and respired carbon in the Eastern Equatorial Pacific over the last deglaciation. *Paleoceanography*, *32*(12), 1371-1385.

Dickson, A. G., & Millero, F. J. (1987). A comparison of the equilibrium constants for the dissociation of carbonic acid in seawater media. *Deep Sea Research Part A. Oceanographic Research Papers*, *34*(10), 1733-1743.

Doss, W., & Marchitto, T. M. (2013). Glacial deep ocean sequestration of CO2 driven by the eastern equatorial Pacific biologic pump. *Earth and Planetary Science Letters*, *377*, 43-54.

Dymond, J., & Collier, R. (1996). Particulate barium fluxes and their relationships to biological productivity. *Deep Sea Research Part II: Topical Studies in Oceanography*, *43*(4-6), 1283-1308.

Dugdale, R. C., & Wilkerson, F. P. (1998). Silicate regulation of new production in the equatorial Pacific upwelling. *Nature*, *391*(6664), 270-273.

Emerson, Steven, and John Hedges. (2008) *Chemical oceanography and the marine carbon cycle*. Cambridge, Eng: Cambridge University Press.

Field, C. B., Behrenfeld, M. J., Randerson, J. T., & Falkowski, P. (1998). Primary production of the biosphere: integrating terrestrial and oceanic components. *Science*, *281*(5374), 237-240.

Fiedler, P. C., & Talley, L. D. (2006). Hydrography of the eastern tropical Pacific: a review. *Progress in Oceanography*, *69*(2-4), 143-180.

Francois, R., Bacon, M. P., Altabet, M. A., & Labeyrie, L. D. (1993). Glacial/interglacial changes in sediment rain rate in the SW Indian sector of Subantarctic waters as recorded by 230Th, 231Pa, U, and δ15N. *Paleoceanography*, *8*(5), 611-629.

Galbraith, E., Jaccard, S., Pedersen, T. *et al.* (2007). Carbon dioxide release from the North Pacific abyss during the last deglaciation. *Nature* **449,** 890–893.

Griffith, E. M., & Paytan, A. (2012). Barite in the ocean–occurrence, geochemistry and palaeoceanographic applications. *Sedimentology*, *59*(6), 1817-1835.

Hertzberg, J. E., Schmidt, M. W., Bianchi, T. S., Smith, R. W., Shields, M. R., & Marcantonio, F. (2016). Comparison of eastern tropical Pacific TEX86 and Globigerinoides ruber Mg/Ca derived sea surface temperatures: Insights from the Holocene and Last Glacial Maximum. *Earth and Planetary Science Letters*, *434*, 320-332.

Jaccard, S. L., Galbraith, E. D., Martinez-Garcia, A., & Anderson, R. F. (2016). Covariation of deep Southern Ocean oxygenation and atmospheric CO 2 through the last ice age. *Nature*, *530*(7589), 207-210.

Jaccard, S. L., Galbraith, E. D., Sigman, D. M., Haug, G. H., Francois, R., Pedersen, T. F., ... & Thierstein, H. R. (2009). Subarctic Pacific evidence for a glacial deepening of the oceanic respired carbon pool. *Earth and Planetary Science Letters*, *277*(1-2), 156-165.

Johnsen, S. J. & North Greenland Ice Core Project members, High-resolution record of Northern Hemisphere climate extending into the last interglacial period. *Nature* **431**, 147–151 (2004).

Koutavas, A., & Lynch-Stieglitz, J. (2003). Glacial-interglacial dynamics of the eastern equatorial Pacific cold tongue-Intertropical Convergence Zone system reconstructed from oxygen isotope records. *Paleoceanography*, *18*(4).

Laird, N. P. (1971). Panama Basin deep water properties and circulation. *J. Mar. Res*, *29*(3), 226-234.

Lea, D. W., Pak, D. K., & Spero, H. J. (2000). Climate impact of late Quaternary equatorial Pacific sea surface temperature variations. *Science*, *289*(5485), 1719-1724.

Lea, D. W., Pak, D. K., Belanger, C. L., Spero, H. J., Hall, M. A., & Shackleton, N. J. (2006). Paleoclimate history of Galapagos surface waters over the last 135,000 yr. *Quaternary Science Reviews*, *25*(11-12), 1152-1167.

Le Borgne, R., Feely, R. A., & Mackey, D. J. (2002). Carbon fluxes in the equatorial Pacific: a synthesis of the JGOFS programme. *Deep Sea Research Part II: Topical Studies in Oceanography*, *49*(13-14), 2425-2442.

Loveley, M. R., Marcantonio, F., Lyle, M., Ibrahim, R., Hertzberg, J. E., & Schmidt, M. W. (2017). Sediment redistribution and grainsize effects on 230Th-normalized mass accumulation rates and focusing factors in the Panama Basin. *Earth and Planetary Science Letters*, *480*, 107-120.

Lonsdale, P. (1977). Regional shape and tectonics of the equatorial East Pacific Rise. *Marine Geophysical Researches*, *3*(3), 295-315.

Lonsdale, P., & Malfait, B. (1974). Abyssal dunes of foraminiferal sand on the Carnegie Ridge. *Geological Society of America Bulletin*, *85*(11), 1697-1712.

Lund, D. C., Asimow, P. D., Farley, K. A., Rooney, T. O., Seeley, E., Jackson, E. W., & Durham, Z. M. (2016). Enhanced East Pacific Rise hydrothermal activity during the last two glacial terminations. *Science*, *351*(6272), 478-482.

Marcantonio, F., Hostak, R., Hertzberg, J. E., & Schmidt, M. W. (2020). Deep Equatorial Pacific Ocean Oxygenation and Atmospheric CO 2 Over The Last Ice Age. *Scientific reports*, *10*(1), 1-10.

Martin, J. H., Coale, K. H., Johnson, K. S., Fitzwater, S. E., Gordon, R. M., Tanner, S. J., ... & Barber, R. T. (1994). Testing the iron hypothesis in ecosystems of the equatorial Pacific Ocean. *Nature*, *371*(6493), 123-129.

Martínez-Botí, M. A., Marino, G., Foster, G. L., Ziveri, P., Henehan, M. J., Rae, J. W., ... & Vance, D. (2015). Boron isotope evidence for oceanic carbon dioxide leakage during the last deglaciation. *Nature*, *518*(7538), 219-222.

McManus, J., Berelson, W. M., Klinkhammer, G. P., Hammond, D. E., & Holm, C. (2005). Authigenic uranium: relationship to oxygen penetration depth and organic carbon rain. *Geochimica et Cosmochimica Acta*, *69*(1), 95-108.

McManus, J., Berelson, W. M., Klinkhammer, G. P., Johnson, K. S., Coale, K. H., Anderson, R. F., ... & McCorkle, D. C. (1998). Geochemistry of barium in marine sediments:

Implications for its use as a paleoproxy. *Geochimica et Cosmochimica Acta*, *62*(21-22), 3453-3473.

Mehrbach, C., Culberson, C. H., Hawley, J. E., & Pytkowicx, R. M. (1973). Measurement of the apparent dissociation constants of carbonic acid in seawater at atmospheric pressure 1. *Limnology and Oceanography*, *18*(6), 897-907.

Nürnberg, D., Bijma, J., & Hemleben, C. (1996). Assessing the reliability of magnesium in foraminiferal calcite as a proxy for water mass temperatures. *Geochimica et Cosmochimica Acta*, *60*(5), 803-814.

Pennington, J. T., Mahoney, K. L., Kuwahara, V. S., Kolber, D. D., Calienes, R., & Chavez, F. P. (2006). Primary production in the eastern tropical Pacific: A review. *Progress in oceanography*, *69*(2-4), 285-317.

Pichevin, L., Reynolds, B. C., Ganeshram, R. S., Cacho, I., Pena, L., Keefe, K., & Ellam, R. M. (2009). Enhanced carbon pump inferred from relaxation of nutrient limitation in the glacial ocean. *Nature*, *459*(7250), 1114-1117.

Rae, J. W., Foster, G. L., Schmidt, D. N., & Elliott, T. (2011). Boron isotopes and B/Ca in benthic foraminifera: Proxies for the deep ocean carbonate system. *Earth and Planetary Science Letters*, *302*(3-4), 403-413.

Robinson, R. S., Martinez, P., Pena, L. D., & Cacho, I. (2009). Nitrogen isotopic evidence for deglacial changes in nutrient supply in the eastern equatorial Pacific. *Paleoceanography*, *24*(4).

Schlitzer, R. (2015). Ocean data view.

Schmidt, M. W., Chang, P., Hertzberg, J. E., Them, T. R., Ji, L., & Otto-Bliesner, B. L. (2012). Impact of abrupt deglacial climate change on tropical Atlantic subsurface temperatures. *Proceedings of the National Academy of Sciences*, *109*(36), 14348-14352.

Sigman, D. M., & Boyle, E. A. (2000). Glacial/interglacial variations in atmospheric carbon dioxide. *Nature*, *407*(6806), 859-869.

Stuiver, M., Reimer, P. J., & Braziunas, T. F. (1998). High-precision radiocarbon age calibration for terrestrial and marine samples. *radiocarbon*, *40*(3), 1127-1151.

Stuiver, M., Reimer, P. J., & Reimer, R. W. (2005). CALIB 7.1, Radiocarbon calibration program.

Takahashi, T., Sutherland, S. C., Sweeney, C., Poisson, A., Metzl, N., Tilbrook, B., ... & Olafsson, J. (2002). Global sea–air CO2 flux based on climatological surface ocean pCO2, and seasonal biological and temperature effects. *Deep Sea Research Part II: Topical Studies in Oceanography*, *49*(9-10), 1601-1622.

Takahashi, T., Sutherland, S. C., Wanninkhof, R., Sweeney, C., Feely, R. A., Chipman, D. W., ... & Watson, A. (2009). Climatological mean and decadal change in surface ocean pCO2, and net sea–air CO2 flux over the global oceans. *Deep Sea Research Part II: Topical Studies in Oceanography*, *56*(8-10), 554-577.

Talley, L. D. (2007). *Hydrographic atlas of the world ocean circulation experiment (WOCE): Volume 2: Pacific Ocean*. Southampton: WOCE International Project Office.

Thomson, J., Wallace, H. E., Colley, S., & Toole, J. (1990). Authigenic uranium in Atlantic sediments of the last glacial stage—a diagenetic phenomenon. *Earth and Planetary Science Letters*, *98*(2), 222-232.

Tsuchiya, M., & Talley, L. D. (1998). A Pacific hydrographic section at 88° W: Water-property distribution. *Journal of Geophysical Research: Oceans*, *103*(C6), 12899-12918.

Umling, N. E., & Thunell, R. C. (2017). Synchronous deglacial thermocline and deep-water ventilation in the eastern equatorial Pacific. *Nature communications*, *8*(1), 1-10.

Umling, N. E., & Thunell, R. C. (2018). Mid-depth respired carbon storage and oxygenation of the eastern equatorial Pacific over the last 25,000 years. *Quaternary Science Reviews*, *189*, 43-56.

Wang, Y. J., Cheng, H., Edwards, R. L., An, Z. S., Wu, J. Y., Shen, C. C., & Dorale, J. A. (2001). A high-resolution absolute-dated late Pleistocene monsoon record from Hulu Cave, China. *Science*, *294*(5550), 2345-2348.

Yu, J., & Elderfield, H. (2007). Benthic foraminiferal B/Ca ratios reflect deep water carbonate saturation state. *Earth and Planetary Science Letters*, *258*(1-2), 73-86.

Yu, J., Foster, G. L., Elderfield, H., Broecker, W. S., & Clark, E. (2010). An evaluation of benthic foraminiferal B/Ca and δ11B for deep ocean carbonate ion and pH reconstructions. *Earth and Planetary Science Letters*, *293*(1-2), 114-120.

VITA

Brian James Close

Education

December 2020 **M.S., Ocean & Earth**
Old Dominion University, 4402 Elkhorn Ave, Norfolk, VA

August 2017 **B.S., Geology**
West Virginia University, 98 Beechurst Ave, Morgantown, WV

HONORS AND AWARDS

Dorothy Brown Smith Travel Award Fall 2019

Old Dominion University President's List Spring 2019
Fall 2018

Old Dominion University Dean's List Fall 2019
Spring 2018

West Virginia University Dean's List Fall 2016
Spring 2015
Spring 2014

Conference Presentations

American Geophysical Union Fall 2019 meeting
San Francisco, CA

Poster Title: "Refining the depth and location of the respired carbon pool in the tropical Equatorial Pacific over the last 25 kyr using benthic B/Ca"

Leadership Positions

Lead Geology Teaching Assistant
Ocean, Earth, and Atmospheric Science Dept.
Old Dominion University, Norfolk, VA

Event Coordinator
Ocean, Earth, and Atmospheric Science Dept. GSO
Old Dominion University, Norfolk, VA